Design and Control of a Bio-Inspired Human-Friendly Robot

Dongjun Shin[1] Irene Sardellitti[3] Yong-Lae Park[2] Oussama Khatib[1] and Mark Cutkosky[2]

[1] Artificial Intelligence Laboratory, Stanford University, USA
{djshin, ok}@robotics.stanford.edu
[2] Mechanical Engineering, Stanford University, USA
{ylpark, cutkosky}@stanford.edu
[3] ARTS Lab., Scuola Superiore Sant'Anna, Italy irene@arts.sssup.it

Summary. The increasing demand for physical interaction between humans and robots has led to the development of robots that guarantee safe behavior when human contact occurs. However, attaining established levels of performance while ensuring safety poses formidable challenges in mechanical design, actuation, sensing and control. To achieve safety without compromising performance, the human-friendly robotic arm has been developed using the concept of hybrid actuation. The new design employs inherently-safe pneumatic artificial muscles augmented with small electrical actuators, human-bone-inspired robotic links, and newly designed distributed compact pressure regulators with proportional valves. The experimental results show that significant performance improvement that can be achieved with hybrid actuation over a system with pneumatic artificial muscles alone. The paper evaluates the safety of the new robot arm and demonstrates that the safety characteristics surpass those of previous human-friendly robots.

1 Introduction

There is a growing interest in human-friendly robotics involving close physical interaction between robots and humans. With the ability to support a variety of commercial uses, applications for human friendly robots have emerged in medicine, home care, manufacturing and entertainment. A major challenge in such applications is safety: How can robots be sufficiently fast, strong, and accurate to do useful work while also being inherently safe for physical interaction?

Robots have traditionally relied on electromagnetic actuators, which offer excellent controllability but poor power-to-weight ratios compared to pneumatic muscles. Even more limiting is their inability to exert large sustained forces without high transmission ratios between the motor and the load. The high transmission ratios result in robot arms with high mechanical impedance,

which are inherently less safe than their biological counterparts when unexpected contacts occur. Previous efforts to increase the safety of robot arms while maintaining control performance have included relocating the actuators to the base and powering the joints with cables [9, 4], designing links with high-strength composite materials to minimize inertia [1], and employing a series elastic actuator [8]. Other works have employed variable compliance [2] and/or compliant, energy-absorbing layers and proximity sensors to detect impending collisions [6].

1.1 Previous work

Distributed Macro-Mini (DM^2) actuation provides a combination of high power, low impedance, and precise control as shown in the Fig. 1 (a) [11]. Large (macro), low frequency actuators are located at the base of the robot arm as the main source of mechanical power; mini actuators are located at the joints for fast response. Although the DM^2 design approach achieves a significant increase in the control bandwidth and reduction in the effective inertia, the poor power density of electrical actuators still requires high gear ratios, which result in a heavy and bulky system. Furthermore, cable transmissions increase the complexity of the design and assembly.

To address these design issues, the Stanford Safety Robot, $S2\rho$, employs hybrid actuation, combining powerful pneumatic actuators with small electrical actuators in a parallel configuration at each joint as shown in Fig. 1 (b) [10]. Key features embodied in the $S2\rho$ include: replacement of heavy electrical actuators with compliant pneumatic muscles; utilization of compact pressure regulators within the links; and integration of valves, actuators and electronics around a sculpted, bone-like structural element. The pneumatic muscle enables the prototype arm to be light, compact, and compliant due to its high force-to-weight ratio and air compressibility. The distributed compact pressure regulators decrease air flow resistance and reduce the complexity of

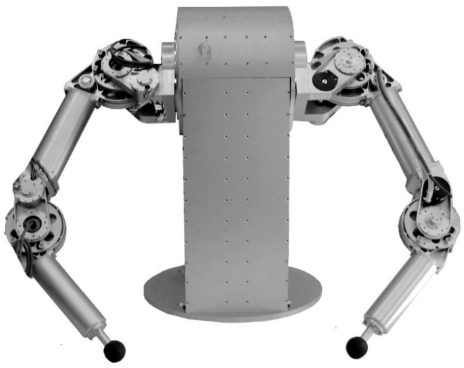

(a) 3DOF Human Friendly Robot

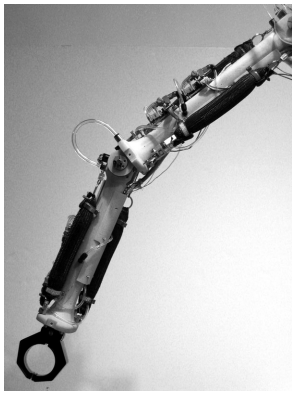

(b) First-generation $S2\rho$

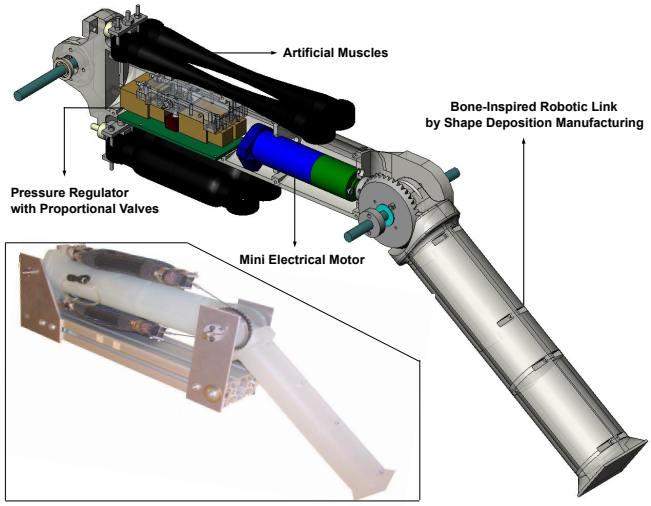

Fig. 1. New Stanford Safety Robot (a new 1-DOF prototype)

the arm by being located adjacent to the actuators. The human-bone-inspired robotic link further reduces the inertia and simplifies design and manufacturing. However, the discovered limitations of the $S2\rho$ robotic arm are as follows: a restricted joint motion and torque that result from limited contraction ratio of the artificial muscles; relatively slow pneumatic response caused by restricted air flow rates in the valves; and limited strength-to-weight ratios for the bone structures.

1.2 New Approach

The second-generation $S2\rho$ addresses some of the discovered limitations. The new design incorporates multiple parallel pneumatic actuators at each joint to increase the range of motion and available torque without becoming bulky. The actuators are controlled by a new proportional valve system for fast response and smooth force control. The valves, along with the mini actuators and other components, are housed in a new thin-walled structure that provides a combination of light weight and robustness. The results of our continuing experimentation and redesign on new $S2\rho$ are shown in Fig. 1.

This paper presents the details of the actuation and robotic structure of the new $S2\rho$ in Section 2. The control strategy and design process are described in Section 3, followed by experimental and analytical results in Section 4. Finally, the paper provides a conclusion and discussion of future work in Section 5.

2 Design

The first-generation $S2\rho$ robotic arm uses a single pair of McKibben artificial muscles as macro actuators, taking advantage of their high power/weight ratio and intrinsic compliance. A limitation of McKibben muscles is that they have a modest ($\approx 22\%$) contraction ratio, and thus provide the limited range of motion. To overcome this problem, the new design (Fig. 1) uses multiple muscles in parallel on each side of the pulley to provide a higher force without excessive bulk and without excessive time to fill and exhaust the muscle chambers. Using the same 40.6 mm pulley for a maximum torque of 8.12 Nm, the new configuration achieves 127 degrees of rotation.

Compact valves in the former robotic arm result in a performance limitation in transient and steady-state operation. The restricted flow rate (orifice size: $0.5mm$) causes substantial errors in transient response. In addition, their on-off behavior produces undesirable overworking and/or oscillation in steady-state operation, especially at high pressure. The new design exploits valves (MD Pro, Parker) with higher flow rates (orifice size: $1.427mm$) and a proportional flow control feature. The proportional valves achieve a significantly faster initial response and a faster convergence to the desired pressure.

The first-generation $S2\rho$ robotic arm used a polymer structure as the central bone-like support. The structure was created using selective laser sintering (SLS) with a glass-filled nylon. While SLS allows almost arbitrary shapes to be realized, the resulting parts are not particularly strong for their weight. The new arm is created using SDM, which allows combinations of hard and soft materials, as well as sensors and other discrete parts, to be integrated in a single heterogeneous structure. The new link is a thin-walled shell (Task 9, Shore 85D polyurethane) that houses the valves, mini actuator, controllers and wiring. To create a conduit for the cable that is pulled by the Mckibben actuators, a hollow nylon tube was embedded in the pulley, and part of it was removed as shown in Fig. 2.

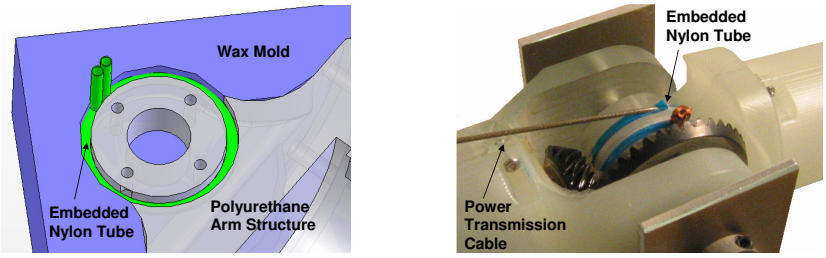

(a) SDM process for nylon tube (b) Embedded nylon tube for cable

Fig. 2. To create a conduit for the cable that is pulled by the Mckibben actuators, a hollow nylon tube was embedded in the pulley, and part of it was removed.

3 Control Strategy

The $S2\rho$ robotic arm is controlled employing a pair of actuators, connected in parallel. The controller partitions the reference input torque between the low frequency actuation (macro actuation) and the high frequency actuation (mini actuation) based on the frequency. For low frequency actuation, low impedance output is achieved by using the light pneumatic muscles. For high frequency actuation, low impedance is achieved by using a small low-inertia motor connected to the manipulator through a low-friction, low-reduction cable transmission. This results in reducing the weight of the moving arm drastically, while the on-joint mini actuator increases the control bandwidth and fast dynamics.

3.1 Macro Actuation

The macro actuator is an antagonistic pair of pneumatic muscles as shown in Fig. 3 (a). When a desired torque is to be produced for the joint, the necessary force difference is symmetrically distributed between the two antagonistic muscles and controlled by force feedback, which closes the control loop around the pneumatic muscles through load cell measurements as shown in Fig. 5 (a). The force feedback compensates for the pneumatic muscle force/displacement hysteresis phenomenon while also increasing the actuation bandwidth. The macro actuation system is identified as a second-order system at the joint angle, q of 1.94^o, as shown in Fig. 3 (b).

However, experiments with respect to different configurations, which are associated with joint angle, demonstrate that muscle dynamics depend on

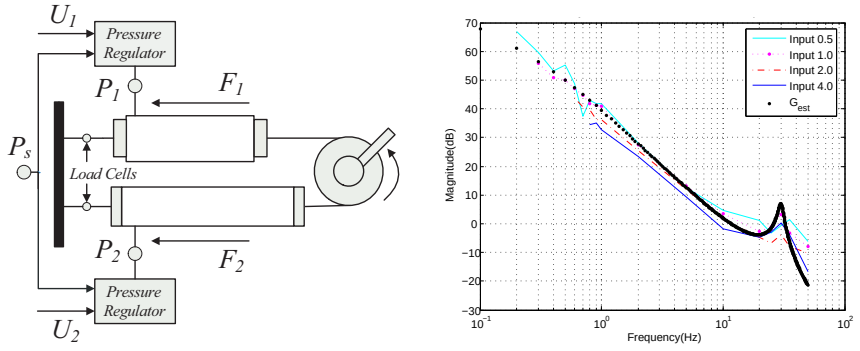

(a) Macro Actuation Schematic (b) Macro System Identification

Fig. 3. (a) Macro Actuation, which consists of regulator and muscles. $P_1(P_2)$, $U_1(U_2)$, $F_1(F_2)$ and P_s denote regulated muscle pressures, muscle forces, command signal and supply pressure, respectively. (b) Estimated bode plot of the macro actuation system. For an input of 4 V, the system deviates from the predicted bode plot due to saturation of the pressure regulator.

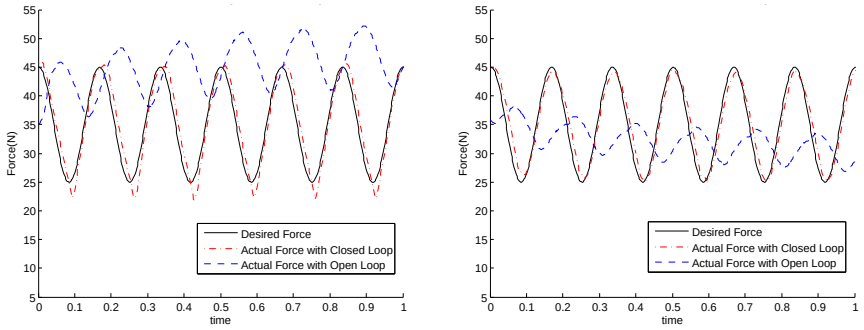

(a) Macro Force Control at $q = 1.94^o$ (b) Macro Force Control at $q = 29.80^o$

Fig. 4. Macro Force control comparison for open-loop and closed loop control at 6Hz, the bandwidth of the macro closed loop force control . Fig. (a) and (b) demonstrate the force feedback PID control tracks the reference input consistently regardless of the muscle length, while the open-loop control shows significant deviation from reference input command and different behavior depending on the muscle length.

muscle length. It means the system gain changes with respect to muscle length, while the system order is maintained. The system gain with respect to the joint angle is fit with a cubic spline:

$$K = -4.2 \times 10^{-4} q^3 + 7.4 \times 10^{-3} q^2 + 1.5q + 97 \tag{1}$$

Based on the previously described system identification, PID controller with adaptive gain in continuous time domain is given by

$$C = \frac{22.5}{K} \frac{s+6}{s+300} \frac{s+25}{s+0.01} \tag{2}$$

where, K is the equation (1).

The closed loop PID control with adaptive force feedback through load cell significantly improves force control performance over the open-loop control that uses the pneumatic muscle analytical model alone. As shown in Fig. 4, the closed loop PID control works successfully at 6Hz, the bandwidth of the macro closed loop force control, while the open-loop control shows significant deviation from reference input command.

3.2 Hybrid Actuation

The hybrid actuation control scheme adopts dual actuation with macro and mini actuation. The hybrid actuation controller separates commanded torques into the macro, i.e., pneumatic muscles, and the mini, i.e., electrical motor, on the basis of frequency content. The torque applied on the joint will then be the linear combination of the macro and mini torque contributions, as shown in Fig. 5 (b). For the mini controller, an open-loop torque controller

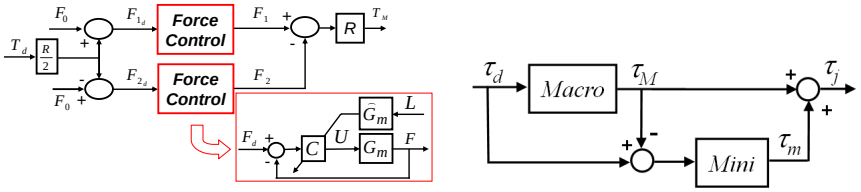

(a) Macro Torque Control with Adaptive Force Control

(b) Hybrid Actuation

Fig. 5. (a) The block, Force Control, represents an individual muscle adaptive force controller. The compensator gain of macro force control is adapted with respect to the configuration. R and L denote the radius of the pulley and the length of muscle, respectively. (b) The torque applied on the joint is the linear combination of the macro and mini torque contributions.

is implemented. The measured torque error of the macro actuation is directly commanded to the mini actuation. Mechanical advantages such as low gear reduction ratio and near-collocated actuator allow us to assume that the desired torque of the mini actuation is achieved at the joint. The faster dynamics of the mini actuation compensate for the slow dynamics of the macro actuation.

4 Experimental Results

In order to validate the hybrid actuation concept for the human friendly robot, we built a one-degree-of-freedom testbed as explained in Sec. 2 and shown in Fig. 1. For performance analysis, open-loop contact force tests with hybrid actuation and position control with hybrid actuation were conducted. For safety analysis, the normalized effective mass was simulated and compared to other robotic arms.

4.1 Performance Characteristics

Measuring and analyzing open-loop contact forces at the end effector enables validation of the force/torque control using hybrid actuation. Fig. 6 (a) shows the performance difference between the macro actuation alone and hybrid actuation. Hybrid actuation achieves a force control bandwidth of 26Hz while macro actuation achieves 6Hz. A negligible steady state error of contact force with hybrid actuation demonstrates that open-loop torque control is satisfactory for the mini actuator.

In addition, position tracking experiments were conducted for the macro actuation and the hybrid actuation. In Fig. 6 (b), the position tracking error of the macro and the hybrid actuation are plotted for a sinusoidal reference

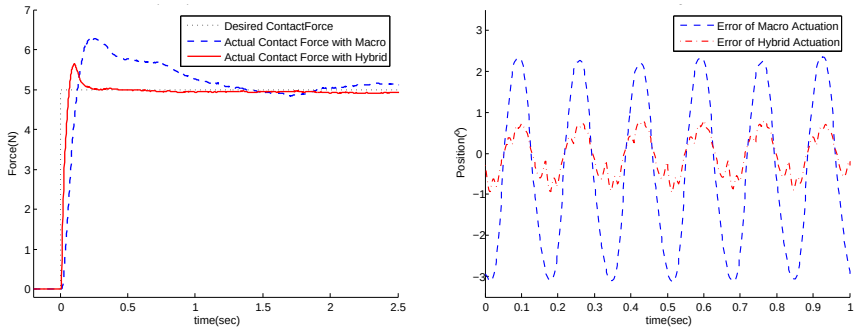

(a) Contact Force Control (b) Position Control Error

Fig. 6. (a) Open-loop contact force control comparison for macro and hybrid control. Hybrid actuation achieves a bandwidth of 26Hz while macro actuation achieves 6Hz. (b) Position tacking error comparison for macro and hybrid control with a sinusoidal reference input (10 degrees at 6Hz).

input, of which frequency is 6Hz and amplitude is 10^o. The result shows that the hybrid actuation control shows significant performance improvement over the macro actuation alone in compensating for the non-linear effect of the pneumatic muscles. In addition, the results demonstrate that the new design and control scheme of $S2\rho$ overcomes the performance limitations of the first-generation $S2\rho$, for which the position control bandwidth was 2Hz [10].

4.2 Safety Characteristics

To demonstrate the safety of the proposed robot arm design in reducing the impact impulse, we simulated the effective mass/inertia. Fig. 7 (a) displays the effective mass at the same shoulder and elbow configurations for a PUMA560, the DM^2 and $S2\rho$. The diagram demonstrates that the effective hybrid actuation approach reduces the effective mass by approximately a factor of two compared to the previous DM^2. The $S2\rho$ robotic arm has a maximum effective mass of 1.4kg as compared to 3.5kg for DM^2, while a conventional robot such as PUMA560 has the far greater effective mass of 25kg.

However, a lower effective mass may come at the expense of reduced performance if the lower effective mass is a consequence of using lower gear ratios and smaller actuators. Therefore, the safety analysis needs to incorporate additional constraints that enable comparisons among manipulators at the same level of performance. As shown in the Fig. 7 (b), the effective mass of each robotic arm is normalized by its own payload, so that the safety comparison between robotic arms with different size/payload can be made. While the PUMA560 and DM^2 have normalized effective masses of 1.154 and 0.058, $S2\rho$ shows only 0.015. The improved result compared to the previous DM^2 approach shows that the safety of $S2\rho$ is not compromised by an additional

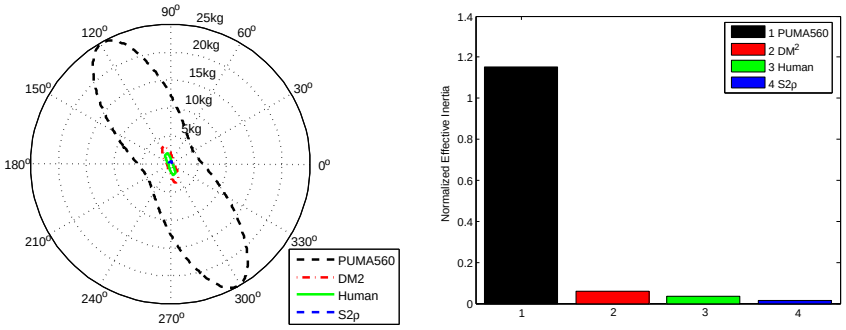

(a) Effective Mass (b) Normalized Effective Mass

Fig. 7. (a) Effective mass of DM^2, S2ρ and Human. S2ρ has a maximum effective mass of 1.4kg as compared to 3.5kg for DM^2 and 2.2kg for the Human, while the conventional PUMA560 has an effective mass of 25kg. (b) Normalized effective Inertia. Effective inertia is normalized by payload for better comparison. The PUMA560 has a normalized effective mass of 1.15 but S2ρ shows only 0.015.

actuator, i.e., the pneumatic muscle. For an additional comparison, we provide the normalized effective mass of an average U.S. male civilian arm, which is sampled from surveys of U.S. populations [3, 5].

5 Conclusion and Future Work

The concept of hybrid actuation is presented with a revised version of the Stanford Safety Robot Arm, referred as to S2ρ. Additional pneumatic muscles connected in parallel provide a wider range of motion without sacrificing the joint torque and response time. New pressure regulators with proportional valves improve the response time in transient conditions and reduce steady state errors. A new manufacturing method, Shape Deposition Manufacturing, enables the integration of power sources as well as mechanical components so that the system can be lighter, stronger and more compact. A PID force feedback control with the load cell improves the performance of macro actuation and confirms the system identification for various muscle conditions. Used in combination with open-loop torque control for the mini actuator, the hybrid system shows significant performance improvement over the arm with pneumatic actuation alone. Safety simulations using the normalized effective mass/inertia validate the arm safety characteristics, which are comparable to those of a human arm.

In terms of design, ongoing work is concerned with incorporating force sensors into the structure and covering it with a compliant skin, as part of our extended effort to create powerful, responsive, human-safe robots. Future

versions of the robot arm structure will include fiber reinforcement for higher specific strength and embedded sensors to measure loads on the arm, following the approach used in [7]. The arm will also be covered with a compliant skin with embedded sensors communicating over a network. In terms of control, the analysis of stiffness characteristics and interference between macro and mini actuation will be conducted.

6 Acknowledgements

The authors gratefully acknowledge the support of General Motors. In addition, the authors would like to appreciate the strong contribution of Marc Strauss at Artificial Intelligence Laboratory, Stanford University.

References

1. A. Albu-Schaffer and G. Hirzinger. State feedback controller for flexible joint robots: A globally stable approach implemented on dlr's lightweight robots. *Proc. of the 2000 IEEE/RSJ International Conf. on Intelligent Robots and Systems*, 2:1087–1094, 2000.
2. A. Bicchi and G Tonietti. Fast and soft arm tactics: Dealing with the safety-performance trade-off in robot arms design and control. *IEEE Robotics and Automation Magazine*, 11:22–33, 2004.
3. D. Chaffin, G. Andersson, and B. Martin. Occupational biomechanics. *Fourth Edition, Wiley*, 2:47–49, 2006.
4. J. B. Morrel. Parallel coupled micro-macro actuators. *PhD thesis, Massachusetts Institute of Technology, Cambridge, MA*, 1996.
5. NASA. Man-systems integration standards. *NASA-STD-3000*, 1:Section 4, 1995.
6. J.L. Novak and I.T. Feddema. A capacitance-based proximity sensor for whole arm obstacleavoidance. *Proc. of the 1992 IEEE International Conference on Robotics and Automation*, 2:1307–1314, 1992.
7. Y-L. Park, K. Chau, R. J. Black, and M. R. Cutkosky. Force sensing robot fingers using embedded fiber Bragg grating sensors and shape deposition manufacturing. *Proc. of the 2007 IEEE International Conference on Robotics and Automation*, pages 1510–1516, 2007.
8. G. Pratt and Williamson M. Series elastic actuators. *Proc. of the 1995 IEEE/RSJ International Conference on Intelligent Robots and Systems*, 1:399–406, 1995.
9. J.K. Salisbury, B.S. Eberman, W.T. Townsend, and M.D. Levin. Design and control of an experimental whole-arm manipulator. *Proc. of the 1989 International Symposium on Robotics Research*, 1989.
10. D. Shin, I. Sardellitti, and O. Khatib. A hybrid actuation approach for human-friendly robot design. *to appear in Proc. of the 2008 IEEE International Conference on Robotics and Automation*, 2008.
11. M. Zinn, O. Khatib, B. Roth, and J. K. Salisbury. Towards a human-centered intrinsically-safe robotic manipulator. *Proc. of the 2002 IARP/IEEE-RAS Joint Workshop, Toulouse, France*, 2002.